Chemical Engineering Science 79 (2012) 138–152

Contents lists available at SciVerse ScienceDirect

Chemical Engineering Science

journal homepage: www.elsevier.com/locate/ces

Two-phase air–water flow through a large diameter vertical 180° return bend

M. Abdulkadir [a], D. Zhao [a], A. Azzi [b], I.S. Lowndes [a], B.J. Azzopardi [a,*]

[a] Process and Environmental Engineering Research Division, Faculty of Engineering, University of Nottingham, University Park, Nottingham, NG7 2RD, United Kingdom
[b] Université des Sciences et de la Technologie Houari Boumediene (USTHB), FGMGP, LTPMP, Bab Ezzouar, 16111 Algiers, Algeria

HIGHLIGHTS

- Large scale experiments on gas/liquid flow inverted U bend geometry.
- Time series of fraction of liquid travelling as film.
- Flow pattern identification.
- Criterion for identifying whether liquid on inside and outside of bend.

ARTICLE INFO

Article history:
Received 8 October 2011
Received in revised form
15 May 2012
Accepted 18 May 2012
Available online 2 June 2012

Keywords:
Gas/liquid
Conductance technique
180° bend
Large diameter
Film fraction
Flow regime

ABSTRACT

An experimental study of churn-annular flow behaviour and mean film fraction of an air–water mixture flowing through a vertical 180° return bend using an electrical conductance technique is reported. Measurements were made of film fraction using probes placed before, within the bend (45°, 90°, 135°) and after the bend. The bend, made of transparent acrylic resin, has a diameter of 127 mm and a curvature ratio (*R/D*) of 3. The superficial velocities of air ranged from 3.5 to 16.1 m/s and those for water from 0.02 to 0.2 m/s.

Flow patterns were identified using the characteristic signatures of Probability Density Function (PDF) plots of the time series of mean film fraction. The average film fraction is identified to be higher in the straight pipes than in the bends. The study also identified that at low gas superficial velocity, the film fraction for the riser was generally greater than for the downcomer. For low liquid and higher gas flow rates, film break down occurs at the 45° bend due to gravity drainage. The condition for which the liquid goes to the outside or inside of the bend are identified based on a modified form of Froude number based on published material. A comparison between the present work and that of Hills (1973) based on the mean film fraction showed same tendency.

1. Introduction

The vertical 180° return bends are widely used in waste heat reboilers, nuclear reactors and steam generators, evaporators and heat exchangers. These equipment are significant to increasing the economic efficiency of the plants. The flow usually enters the equipment as a subcooled liquid. Nucleation can start once the wall has achieved a sufficiently high temperature. It is noted that this can occur even though the mean liquid temperature is below the saturation temperature at the operating pressure. The fraction of vapour continues to increase with flow patterns such as churn and annular occurring successively up the tube. If the heat flux is sufficiently high, the liquid film in annular flow can dry out leaving the heater surface covered with a vapour blanket-film boiling. This last event can occur at qualities below 1.0 (100%), the residual liquid would be travelling as drops and effectively insulated from the heater surface by the vapour. Obviously, the important points are the onset of nucleate boiling, heat transfer in the wetted region and the occurrence of the point of dryout.

Liquid distribution and wall shear stress are known to have considerable influence on heat transfer both by affecting directly the heat transfer rate and also by affecting the mechanism by which heat transfer occurs (Hills, 1973). Two extremes are of importance in the latter case: the onset of nucleate boiling and the occurrence of dry wall conditions. Dry wall conditions, also known as dryout can be serious in industrial applications because of the decrease in heat transfer coefficient with the consequent danger of overheating and damage to the pipe. In some applications there is

* Corresponding author. Tel.: +44 115 951 4167; fax: +44 115 951 4181.
E-mail address: barry.azzopardi@nottingham.ac.uk (B.J. Azzopardi).

0009-2509/$ - see front matter © 2012 Elsevier Ltd. All rights reserved.
http://dx.doi.org/10.1016/j.ces.2012.05.029

also the likelihood of solids deposition in the vicinity of the dry patch. If there is an intermittent wetting and drying, corrosion is encouraged. According to Chong et al. (2005), predictions of the occurrences of dryout are vital for the optimal design, in terms of safety, cost and efficiency, of industrial equipment such as boilers, reboilers and heat exchangers.

Considerable effort has been dedicated to flow in straight or inclined small internal diameter pipes. However, real industrial plant units rarely consist entirely of straight pipes and with small internal diameter. According to Conte and Azzopardi (2003), the diameters of pipelines in the oil/gas production industry are usually in the range 0.1–1 m. In that environment, equipment contains numerous fittings such as bends, valves and contractions connected to pipes of large internal diameter.

1.1. Two-phase gas–liquid flow in 180° bends

The flow through vertical and horizontal 180° bends have been investigated experimentally: Oshinowo and Charles (1974), Anderson and Hills (1974), Usui et al. (1980, 1983), Hoang and Davis (1984), Wang et al. (2003, 2004, 2008).

Alves (1954) studied air–water and air–oil flow in a four pass one inch bore horizontal pipeline contactor. Between each pass there was a return bend in a vertical plane, the direction of flow being upwards. The curvature ratio ($R/D=14$). He observed that annular flow, which occurred in the horizontal passes for a superficial gas Reynolds number greater than 40,000, was stable in the bend. Visual observation suggested that the liquid film was probably thicker on the inside of the bend than on the outside.

Oshinowo and Charles (1974) and Usui et al. (1980; 1983) discussed the interaction of the centrifugal force and gravity for the flow about a bend axis qualitatively. Usui et al. (1980, 1983) explained this interaction by proposing a modified form of Froude number expressed in terms of v_L and v_G

$$Fr_\theta = \frac{v_L^2}{\frac{(\rho_L-\rho_G)}{\rho_L} R g \sin\theta}\left\{1-\frac{\rho_G {v_G}^2}{\rho_L {v_L}^2}\right\} \tag{1}$$

where ρ_G and ρ_L are the density of gas and liquid, respectively; v_G and v_L are the actual velocity of gas and liquid, respectively; θ is the angle between the radius and the horizontal; R and g are the radius of the bend and acceleration due to gravity, respectively.

From an evaluation of this expression, the relative positions of the liquid and gas phases across the radial direction of the bend may be estimated, namely: when $Fr_0 > 1$, the liquid phase is in the outside of the bend, $Fr_0 < 1$, is in the inner side. This approach is similar to that proposed by Oshinowo and Charles (1974). This led to a Froude number based on the assumption that the frictional and interfacial forces are negligible when compared to the pressure, centrifugal and gravitational forces. They carried out a force balance on the fluid elements in a direction normal to that of the flow at a point in the bend to yield:

$$\text{pressureforce} + \frac{\rho_L {v_L}^2}{R} - \rho_L g \sin\theta = f_{L\theta} \text{ forliquid} \tag{2}$$

$$\text{pressureforce} + \frac{\rho_G {v_G}^2}{R} - \rho_G g \sin\theta = f_{G\theta} \text{ forgas} \tag{3}$$

where $f_{L\theta}$and $f_{G\theta}$are the net forces and θ is the angle between the radius and the horizontal.

They also assumed that the net forces acting on each phase are equal (Eq. (2)=Eq. (3)), so that

$$\frac{\rho_L {v_L}^2}{R} - \rho_L g \sin\theta = \frac{\rho_G {v_G}^2}{R} - \rho_G g \sin\theta \tag{4}$$

Dividing through by$\rho_L g \sin\theta$, yields

$$\frac{v_L^2}{Rg\sin\theta} - \frac{\rho_G v_G^2}{\rho_L Rg\sin\theta} + \frac{\rho_G}{\rho_L} = 1 \tag{5}$$

This is essentially a sum of Froude numbers for the two phases. With these, they attempted an explanation for flow regime across different bend phase positions. They claimed that if the left-hand side of Eq. (5) is greater than 1, then the liquid will move to the outside of the bend and that if less than 1, the liquid will move inside the bend. They made clear the effects of centrifugal and gravitational forces acting on each phase as a function of average void fraction.

Anderson and Hills (1974) report data on liquid film thickness, axial pressure profiles, gas velocity distribution, and droplet entrainment when air and water flowed concurrently in the annular flow regime in a bend mounted in a vertical plane at the top of a straight vertical tube. The diameter and radius of curvature of the bend they used were 25 and 305 mm, respectively. They reported that the behaviour of the liquid film is greatly affected by secondary flows caused by the centrifugal forces in gas. They concluded that an increase in film thickness on the inside of the bend can be attributed to the action of gravity and to the secondary flow existing in the gas phase. They observed a change in flow pattern from annular to stratified flow in the bend at low liquid flow rates. On the other hand, for the high liquid flow rates, local maxima in the film thickness were seen on both the inside and outside of the bend.

Hoang and Davis (1984) utilised needle probes to measure the void fraction along an inverted U-bend in the case of froth flow. This voidage distribution allowed the evaluation of the slip ratio which was found to be greatly increased at the bend exit for low velocity conditions, after which it is diminished slightly in the downstream tube. Later, Takemura et al. (1996) presented experimental results on the flow behaviour, pressure drop characteristics and dryout characteristics by Joule heating for the gas–water two-phase flow through U-shaped and inverted U-shaped bends having a tube diameter of 18 mm. They compared the results obtained from both bends and concluded that for the U-shaped bends, the gas phase flows along the inside of the bend, regardless of the flow rates of gas and water while in an inverted U-shaped bends, at lower gas and liquid flow rates, the tube wall at the outside of the bend in the vicinity of $\theta=120$–150° is covered with gas phase. Also, that the inverted U-shaped bends have a wider safety region against dryout than the U-shaped bends.

Poulson (1991) measured and modelled mass transfer at 180° bends between horizontal tubes under annular two-phase flow conditions using the dissolution of copper in acid ferric chloride solutions. He concluded that mass transfer at bends relative to straight tubes increases with gas superficial velocities and is constant with low liquid superficial velocities. They successfully modelled the effect of bend geometry on mass transfer.

James et al. (2000) investigated the effect of a 90° horizontal bend on two-phase flow using computational and experimental studies. In their simulations using the Eulerian–Lagrangian method, they presented a suggestion as to whether droplets of a given size deposit in the bend. This they achieved by carrying out calculations using droplets of various sizes: 10, 25, 50, 100, 250 and 500 μm diameter.

Sakamoto et al. (2004) carried out experimental work in a horizontal bend attached to a pipe of internal diameter 24 mm using air–water. The conductance type void probe was employed to measure the liquid film thickness and an L-shaped stainless steel sampling tube to measure the local droplet flow rate. They investigated the distributions of annular liquid film thickness and the local drop flow rate in the gas core in a straight pipe and at the end of three U-bends at different angles to the horizontal. They

found out that the local flow rate of droplets in the gas core in horizontal pipe flow reaches a minimum near the lower wall of the pipe and a maximum near the upper wall.

For predicting and thus preventing dryout in serpentine channel of fired reboilers on a hydrocarbon plant, constituted of vertical tubes joined by 180° bends, Chong et al. (2005) proposed a new model which is the extension of the phenomenological model for annular flow in a single vertical channel of Azzopardi (1996). This model was found to confirm adequately the decrease of film flowrate to zero just before the last bend as earlier predicted by Balfour and Pearce (1978) for "C" bends. Balfour and Pearce (1978) conducted an experimental investigation on the distributions of water films and entrained droplets in air–water annular flows in 180° horizontal bend using sampling probes. They took a series of measurements with the probes positioned at 45° intervals around the tube exit and at varying radii. They concluded that in those annular flows where the air speed is high, many of the entrained droplets are thrown very rapidly to the wall and that the entrained fraction tends to zero for high quality annular flows where the films are thin.

A critical review of the literature has revealed that the present state of understanding of two-phase gas–liquid flow in return bends is limited, either concerned with single phase flow or two-phase gas–liquid flow in small diameter pipes with air–water as the model fluids. A summary of papers reviewed involving bends listing experimental conditions and geometries is presented in Table 1. The change of flow structure before and after the bends was mainly obtained by visualization and the underlining mechanism for the change of flow patterns was not discussed. In addition the film fraction is expected to be influenced by the centrifugal and gravity forces along the bend channel. Though, Usui et al. (1983) worked on plug and bubble flows, Anderson and Hills (1974) examined annular flow. Till date no work has been reported on churn flow, the least understood flow pattern. The location at which the film thins out in the bend is very crucial. Its determination is very important as this will establish where insulation can be planned for against flame and when increasing the liquid flow rate above the minimum flow rate for dryout is necessary.

To examine the film fraction behaviour quantitatively in more detail in a pipe with an internal diameter relevant to the oil and gas industry, measurements were made of the film fraction distribution in a 127 mm pipe diameter at: 17 pipe diameter upstream of the bend, 45°, 90° and 135° into the bends, and 21 pipe diameter downstream of the bend. The fluids examined are air and water. The conductance probe method based on the difference of conductivities between air and water was used to evaluate the flow pattern. The flow patterns were determined by analyzing the Probability Density Function (PDF) of the time series of film fraction. The location at which the film thins out in the bend will be determined using a previously published modified form of Froude number. The observations reported in this work on the behaviour of two-phase churn-annular flow on entering a vertical 180° return bend should lead to a deeper understanding of the mechanisms of two-phase flow in specific type of industrial equipment-reboiler.

2. Experimental apparatus

The experimental programme was designed to provide a study of the fluid mechanisms of two phase flow in 180° return bend in

Table 1
Data from experiments involving bends.

Reference	Fluids	Pipe diameter (mm)	Radius of curvature of the bend (mm)	Bend angle and direction	Measured parameters
Alves (1954)	Air-water and air–oil	25.4	356	Horizontal pipeline contactor	Film thickness
Hills (1973)	Air–water	25.4	305	180°, vertical return bend	Film thickness, local drop distribution, gas velocity distribution and axial pressure profiles
Anderson and Hills (1974)	Air–water	25	305	180°, Vertical return bend	Film thickness, Local drop distribution, gas velocity distribution and axial pressure profiles
Oshinowo and Charles (1974)	Air–water	25.4	76.2, 152.4	Serpentine geometry	Void fraction
Balfour and Pearce (1978)	Air – water	25	48.5	180°, Horizontal to horizontal, (upward)	Film thickness
Usui et al. (1980)	Air–water	16 24	90, 132.5 135, 180	180° Horizontal to horizontal (upward)	Void fraction, pressure drop
Usui et al.(1983)	Air–water	24	96	180°, vertical return bend	Local volume fraction
Hoang and Davis(1984)	Air–water	50.8	50.8, 76.2	180° Vertical return bend	Local gas velocity, Void fraction, Bubble size,
Takemura et al. (1986)	Air–water	18	116 435	180° Vertical to vertical.U and inverted U bends	Flow patterns, Pressure drop. Dryout
Poulson (1991)	Air–water	13 22.6	39,95 56.5	180°, Horizontal to horizontal (upward)	Erosion, Mass transfer
James et al. (2000)	Air–water	67.4	300	90° horizontal bend	Drop size
Wang et al. (2003)	Air–water	3, 4.95 and 6.9	9, 14.9, 20.7, 21.3, 35.1, 49.0	180° Horizontal return bend	Flow pattern
Wang et al. (2004)	Air–water	3 and 6.9	9, 20.7, 21.3, 49.0	180° Horizontal return bend	Flow pattern
Sakamoto et al.(2004)	Air–water	24	135	180° Horizontal to horizontal (upward), Vertical upward, 45° upward, Horizontal	Local film thickness, Drop flow rate.
Chong et al. (2005)	Air–water	150	305	Serpentine geometry	Dryout
Wang et al. (2008)	Air–water	3 and 6.9	9, 20.7, 21.3, 49.0	180° vertical return bend	Flow pattern

a vertical plane. The work was limited to those conditions which gave rise to upward churn and annular flows upstream of the bend. The main objective was to investigate the behaviour of the film fraction around the bend, particularly the film fraction variation for flows in specific type of industrial equipment-fired reboiler. It will also look at the occurrence of film breakdown.

2.1. Overview of the experimental facility

The facility used in the present study is shown schematically in Fig. 1. The large close loop facility is located within the Chemical Engineering Laboratories of the University of Nottingham. The test channel, made of plastic pipes with an internal diameter of 127 mm, comprises of a riser, a 180° return bend and a downcomer. The 180° return bend was made by bolting together two slabs of transparent acrylic resin (Perspex) in the surface of which a circular groove with an accurate semi-circular cross-section had been machined. The bend has a radius of curvature of 381 mm ($R/D=3$) while the riser and downcomer lengths are 11 and 9.6 m long, respectively. The bend is of modular construction and a probe can be inserted at 45°, 90° or 135° around the bend as shown in Figs. 1 and 3a. Care has been taken to ensure that there are no discontinuities of diameter at each joint. The probe consists of a pair of metal rings separated by an acrylic resin ring.

In all of the experiments, air and mains tap water at a temperature of 25 °C were used as the test fluids. The liquid and gas superficial velocities employed were in the ranges from 0.02 to 0.2 m/s and 3.5 to 16.1 m/s, respectively. The experiments were carried out at a pressure of 2 bar g. The flow patterns recorded for this range of input flow conditions were churn and annular flows. From an analysis of the data presented in Fig. 2, the transition lines were determined using the mechanistic models suggested by Shoham (2005) and the slug/churn transition of Jayanti and Hewitt (1992). From an analysis of the observations it is concluded that for the churn/annular flow transition, the Shoham transition line is less reliable and in fact under predicts

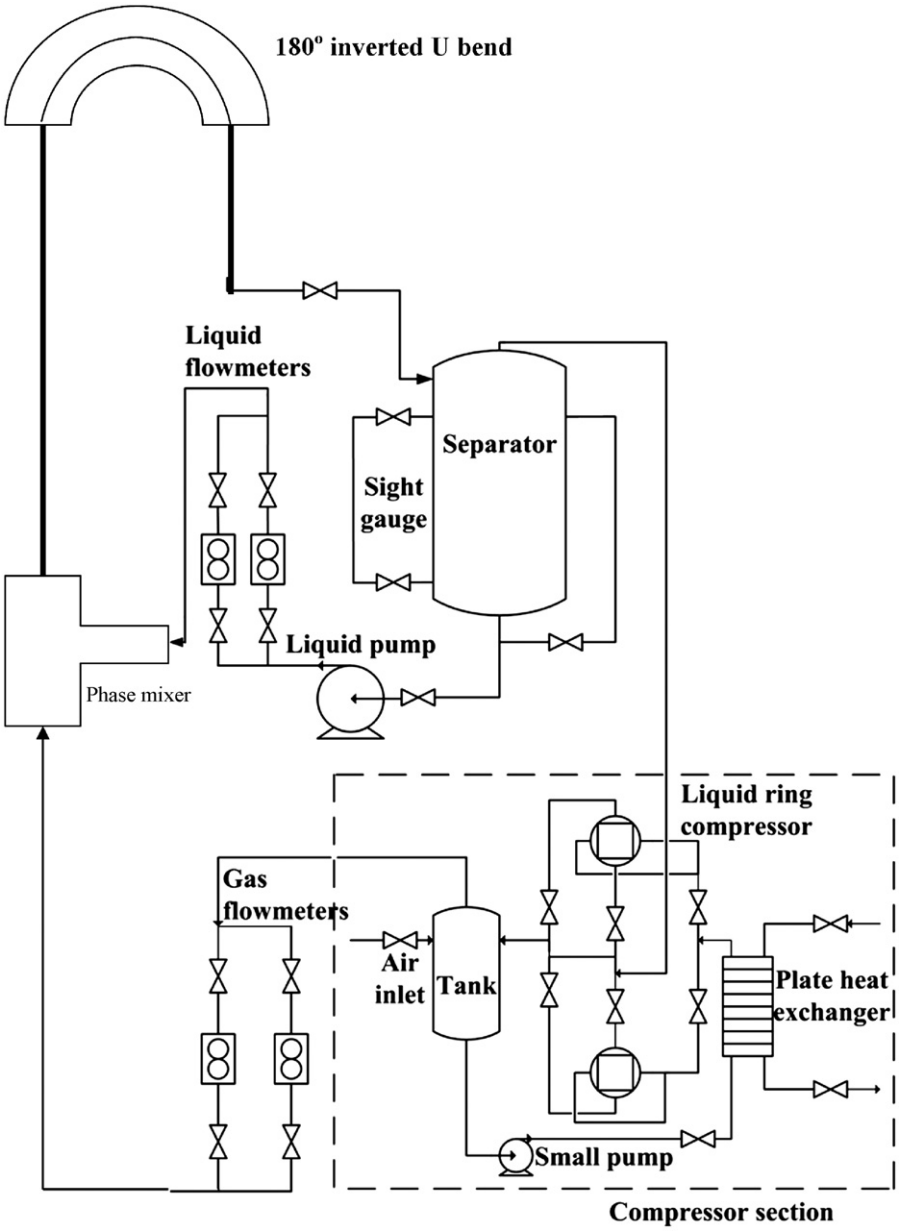

Fig. 1. Schematic diagram of the experimental facility.

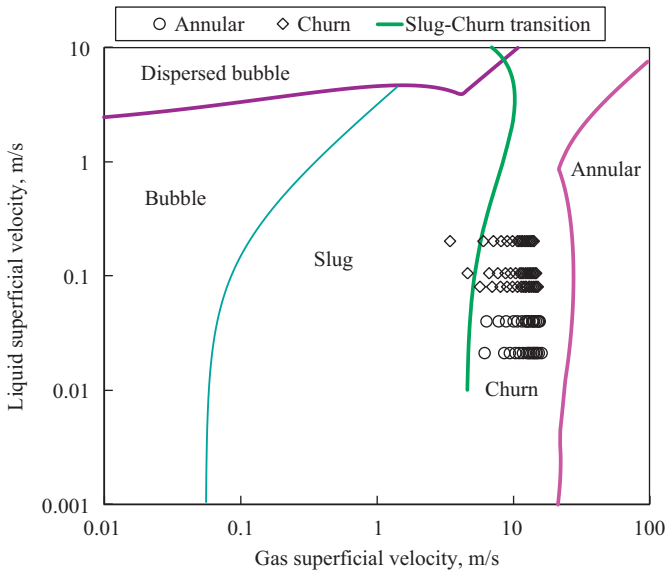

Fig. 2. Flow pattern map for the range of flow rates in the present study.

the conditions examined. On the other hand, the Jayanti and Hewitt transition line performs better, but under predicts the transition from slug/churn flow at higher liquid and lowest gas superficial velocities.

2.1.1. The experimental procedure

Before the start of the experiments, the flow loop was pressurised to 2 bar g using compressed main air. Two liquid ring pumps with 55 kW motors were employed to compress and deliver the air to the mixer. In the mixer, the supplied air combines with the water drawn from the two phase separator/supply tank by means of the centrifugal pump. The mixing device (Fig. 3b) consisted of a 105 mm diameter tube placed at the centre of the 127 mm internal diameter test section, termed an annular injection method. Water enters the main pipe from the periphery to form a uniform film on the pipe wall whilst the air passes along the central pipe. The gas was introduced first to avoid the flooding of the air line with water. The flow rates of the air and water were measured using calibrated vortex and turbine meters, respectively. The temperature and pressure of the system were taken close to the liquid and gas flow meters and at the base of the riser. This allowed the inlet flow rates to the test section for both phases to be determined accurately. The maximum uncertainties in the liquid and gas flow rates according to Omebere-Iyari (2006) are 0.5 and 2.9%, respectively.

Downstream of the mixer, the two-phase mixture travels for 11 m along a 127 mm internal diameter vertical pipe in which annular or churn flow is established. Small inaccuracies in the alignment of a vertical pipe can cause significant asymmetry in the velocity and liquid distribution profiles of multiphase flows (Gill et al., 1963). Consequently, great care was taken to ensure that this tube was true vertical. Indeed, the maximum measured lateral deviation was recorded as little as 1.5°/mm. Along the length of the riser, the time varying cross-sectional film fractions are measured using three identical conductance ring probes placed at distances of 8.1, 8.3 and 8.5 m above the mixer/injection section. These locations correspond to, 64.0, 65.0 and 66.6 pipe diameters above the mixer/injection section.

The test bend, mounted on top of this section is also of a 127 mm internal diameter. Provision was made for the measurement probe to be inserted at every 45° around the bend. Time

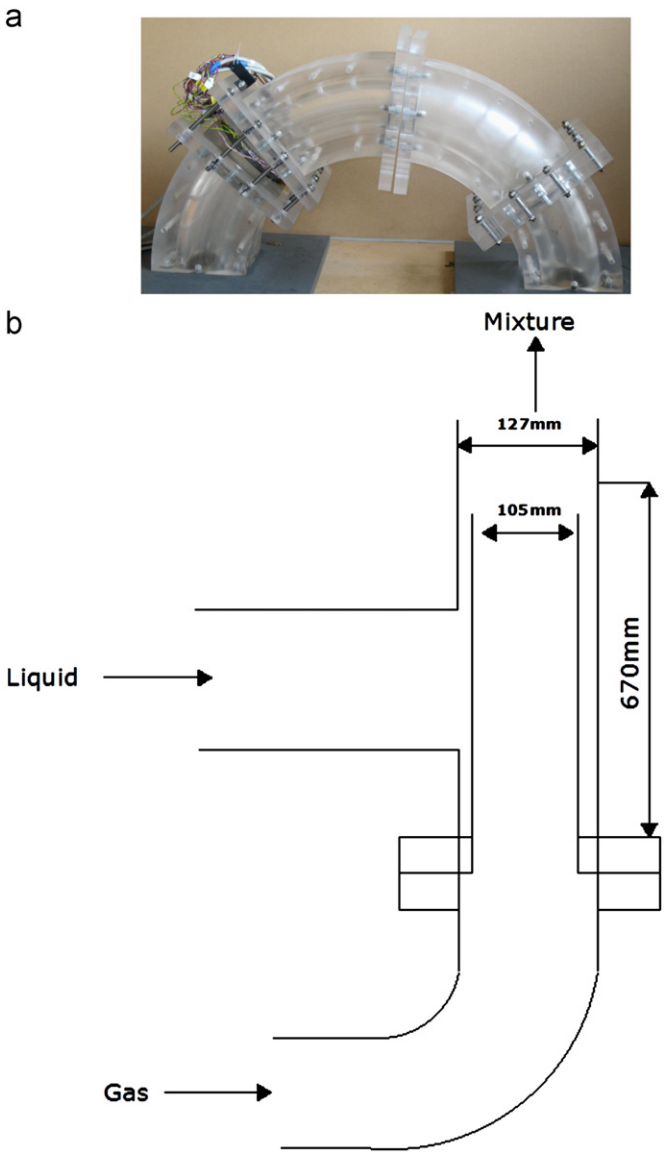

Fig. 3. (a) A 180° return bend and (b) the diagram of the air–water mixing section.

varying cross-sectional film fraction measurements was recorded simultaneously at the three measurement locations in the bend: 45°, 90°, and 135°.

Beyond the bend, the air–water flow mixture travels a further 9.6 m vertically downwards and 1.5 m horizontally to the separator where the gas and the liquid are separated and directed back to the compressors and the pump respectively, to create a double closed loop. As the flow enters the downcomer through the bend, time varying cross-sectional film fractions data is measured using a conductance ring probe placed at 2667 mm (21 pipe diameters) downstream of bend.

2.2. Instrumentation

2.2.1. Film fraction measurement

The film fraction of a gas–liquid flow is a fundamental quantity used in describing the flow pattern; it is the fraction of the pipe cross-sectional area occupied by the liquid phase. Its determination is of great importance in a variety of engineering applications. One of the most common techniques to study the form and the extension of the phase interface consists in measurement of the electrical impedance of the two-phase gas–liquid area close to

a system of electrodes. In such a way, once the relationship between the electrical impedance of the medium and the phase distribution is obtained, the average cross-sectional film fraction can be inferred, depending upon the extension of the measuring region.

Many studies have been carried out on this subject: the main evidence is that the measured electrical impedance across an electrode pair immersed in a conducting liquid is essentially resistive when the frequency of the a.c. excitation signal is sufficiently high (for tap water, 10∼100 kHz) (Fossa 1998). For higher frequencies (above a megahertz) the behaviour of the electrolyte becomes essentially capacitive: for this reason impedance methods are usually classified as either conductance or capacitative methods. With reference to the conductance method, Coney (1973) has reported the theoretical behaviour of flat electrodes wetted by a liquid layer, and Hewitt (1978) has presented a comprehensive critical review of the technique.

In the present work the conductance technique is applied to study two-phase distribution. Air–water mixtures were considered. An a.c. carrier voltage of 10 kHz frequency was applied across each pair of electrodes while an electronic device, especially designed for this purpose, converted the a.c. signal into a d.c. signal proportional to the impedance of the two-phase test section. The frequency was checked to give the resistive behaviour of the water by measuring both the amplitude and phase shift of the applied voltage signal. The detailed description of the design of the probe rings used in the present study has previously been given by Omebere-Iyari (2006). Emphasis was placed on to the repeatability of the measurements and calibration procedures.

2.2.2. Conductance ring probe technique

In air–water churn-annular type flows, the instantaneous wall film thickness can be determined by measurements of the electrical conductance between two electrodes in contact with the liquid film. Different types of electrodes such as flush-wires, parallel wires, flush-mounted pin and ring probes have been adapted (Miya et al., 1971; Brown et al., 1978; Asali and Hanratty, 1985; Andreussi et al., 1988; Koskie et al., 1989; Kang and Kim, 1992; Tsochatzidis et al., 1992; Fossa, 1998; Conte and Azzopardi, 2003). Among these probes, the flush mounted ring probes shown in Fig. 4 is attractive to researchers based on the fact that it provides non-intrusive measurements, can detect small impedance and allows electric field to be effectively confined.

Potential field theory is the basis for flush mounted probes immersed in a two-phase mixture. When electrolytes are subjected to alternating current excitation, their electrical behaviour

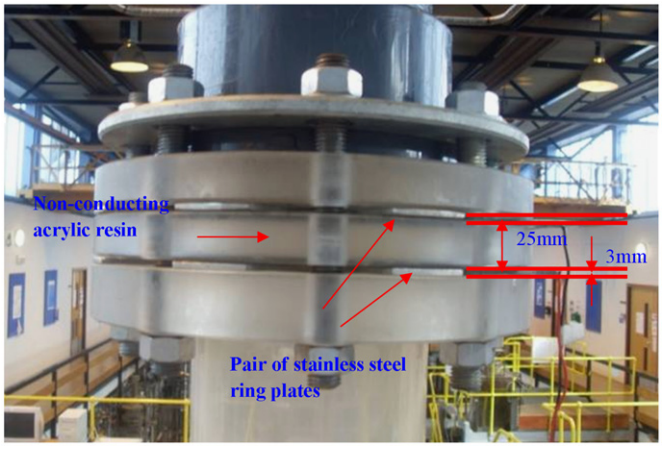

Fig. 4. The conductance ring probe.

is resistive provided the frequency of the applied signal is high enough. The electrical fields of regions with small dimensions when compared to the wavelength of the electric field can be modelled as time invariant (Omebere-Iyari, 2006). The problem is described by the Laplace equation and the electric potential with the proper boundary conditions is:

$$\nabla^2 V = 0 \tag{6}$$

The Laplace equation can then be solved either analytically or numerically depending on the probe geometry and the form of the interface between the phases.

The conductance between two electrodes, Ge, mounted flush all around the perimeter of a pipe of arbitrary cross-sectional area, A, and separated by a distance D_e can be mathematically represented by (Omebere-Iyari, 2006):

$$Ge = \frac{\gamma A}{D_e} H_L \tag{7}$$

where H_L is the fraction occupied by the liquid phase and $\gamma$is the liquid conductivity

Coney (1973) developed a theoretical analysis for predicting the electrical behaviour of rectangular electrodes for short separation distances. Andreussi et al. (1988) found that the dimensionless conductance Ge*, defined as:

$$Ge^* = \frac{Ge}{\gamma L_E} \tag{8}$$

where L_E, is the length of the electrode, could be related to the function of elliptical integrals $k(m)$. The expression for this is:

$$Ge^* = \frac{k(m)}{k(1-m)} \tag{9}$$

with

$$k(m) = \int_0^{\pi/2} (1 - m\sin^2\theta)^{-1/2} d\theta \tag{10}$$

and

$$m = \frac{\sinh^2(\pi s/2h)}{\sinh^2(\pi(s+De)/2h}} \tag{11}$$

Coney's (1973) results were extended by Andreussi et al. (1988) to cover annular and stratified flow configurations for ring electrode. Eq. (8) retains its validity if the electrode length, L_E, is replaced by the wetted length of electrode, P_w. The equivalent layer thickness, h_L is then defined as:

$$h_L = \frac{AH_L}{P_w} \tag{12}$$

where A is the cross sectional area of the duct, H_L is the fraction occupied by the liquid phase and P_w is defined above.

The use of Eq. (9) according to Omebere-Iyari (2006) can be justified by comparing the theoretical predictions with appropriate experimental data. Measurements of the dimensionless conductance, Ge^*, give a convenient experimental procedure from which the film fraction can be determined without prior knowledge of the electrical conductivity of the liquid. The dimensionless conductance is the ratio of conductance at a given film fraction to the conductance when the pipe is full of liquid. This ratio is determined theoretically by combining Eqs. (9) and (12).

A dimensionless parameter Ge^*, is defined as:

$$Ge^* = \frac{R_{full}}{R_x} \tag{13}$$

where R_{full} is when the pipe (test section) is full of liquid, i.e., void fraction=0

Ge^*, the dimensionless or normalised conductance is determined from the voltage response, V_{out}, for every cylinder, and

correlated with the corresponding film fraction. A third order polynomial fit of the form:

$$\text{film fraction} = d + c(Ge^*)^3 + b(Ge^*)^2 + a(Ge^*) \quad (14)$$

is applied to obtain a unique calibration curve for each probe.

Time varying cross-sectional film fraction measurements was made with five identical ring probes located before, in and after the bend. The probes give an output ranging from 0 to 0.32 V, which is proportional to the resistance of the two-phase mixture. They were carefully designed so that the electrodes had the same diameter, D as the test section (127 mm) to ensure flush mounting with the pipe wall. The distance between each pair of stainless steel electrode plates, D_e, and width, S, are 25 and 0.3 mm, respectively. The distances, De and S can be observed in Fig. 4.This results in electrode spacing to pipe diameter ratio (D_e/D) of 0.20 and electrode width to pipe diameter ratio (S/D)=0.024. Data acquisition was performed through a PC equipped with a National Instrument (NI) DAQ card. An existing data acquisition programme in Labview (Omebere-Iyari (2006)) was adapted.

3. Results and discussion

The independent parameters which were measured in this study are the liquid and gas flow rates, the film fraction in both upward and downward flows, as well as 45°, 90° and 135° into the bend. The range over which these parameters were measured is given in Table 2. In total, 102 data points were obtained during the test runs for each of the 45°, 90°, and 135° bend conditions. The uncertainty in film fraction was determined by Omebere-Iyari (2006) according to the principle of Moffat (1988). He found that the estimated absolute error in the film fraction measurement was from 0.018 to 0.027, which corresponds to a relative error of 1.8 to 5% for the majority of the data.

Table 2
The range of variables.

u_{gs} (m/s)	u_{ls} (m/s)	Film fraction	Re_{gs}	Re_{ls}
3.5–16.1	0.02–0.2	0.0–0.2	86,413–402,000	2,535–25,350

3.1. Flow development

Measurements of film fraction obtained from the conductance probes located at the riser were examined to determine the extent of flow development. A fully developed flow is one when the flow pattern does not change with the distance downstream. To achieve this, a comparison of time series, Probabilty Density Function (PDF) and Power Spectral Density (PSD) of film fraction are shown in Fig. 5. Details of the PDF and PSD functions can be found elsewhere, Costigan and Whalley (1997) and Omebere-Iyari (2006).

An examination of Fig. 5(b and c) shows a striking similarity between the shape of the PDF distribution and location of the frequency in the PDF and PSD plots of the three probes at liquid and gas superficial velocities of 0.2 and 14.2 m/s, respectively. The plot of the time series of film fraction (Fig. 5a) for the three locations also did not yield any significant differences. Therefore, there is an indication that equilibrium has been reached and that the flow is fully developed at 64 pipe diameters for the flow condition considered. Interestingly, this is consistent with the results of Omebere-Iyari (2006); he measured the void fraction at various points under similar conditions at 3.5, 30.9, 62.7, 63.8 and 65.5 pipe diameters downstream of the mixer. He found that the variation in the void fraction characteristics at 64 and 65.5 pipe

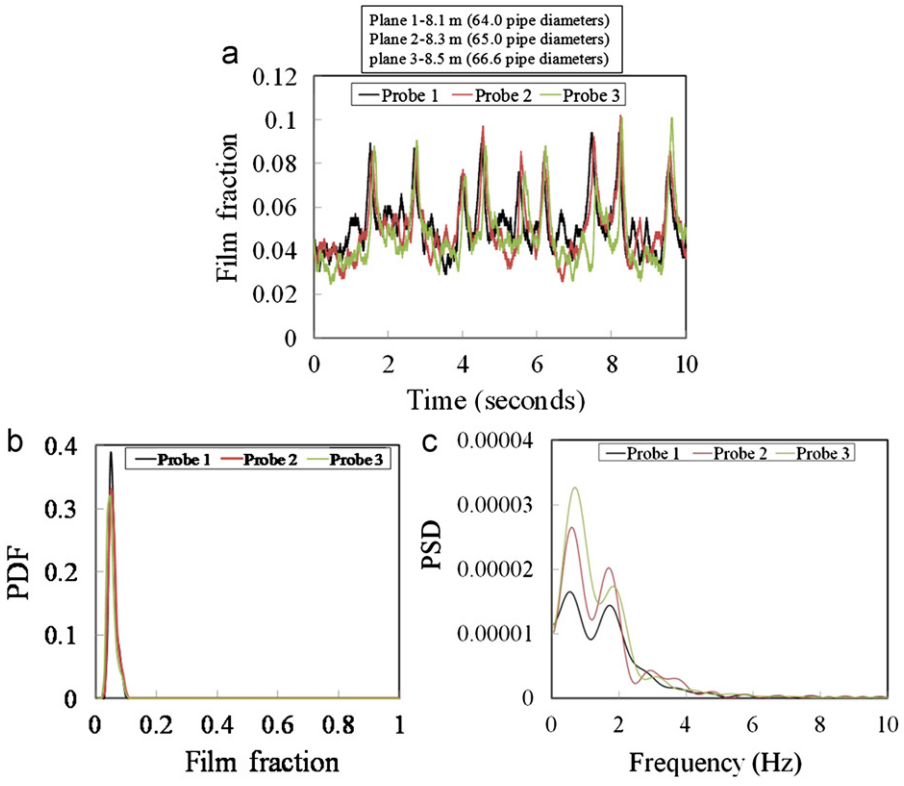

Fig. 5. A typical comparison between the (a) time series of film fraction (b) PDF of film fraction and (c) Power spectral density (PSD) of film fraction obtained at three measurement locations: probes 1, 2 and 3 for liquid and gas superficial velocity of 0.2 and 14.22 m/s, respectively.

diameters were small and concluded that the flow was fully developed at 64 pipe diameters.

3.2. Time series and PDF of dimensionless liquid film thickness, before, around and after the 180° return bend

The time series of film fraction was obtained with the aid of ring conductance probes flush mounted on the pipe. As a result the averaged liquid film thickness for churn and annular type flows were obtained from the relationship (Azzopardi, 2006; Kaji and Azzopardi (2010)) below:

$$\frac{\delta}{D}=\frac{1}{2}\left[1-(\varepsilon_g)^{0.5}\right] \tag{15}$$

Replacing the cross-sectional void fraction, ε_g with ε_F and noting that $\varepsilon_g+\varepsilon_F=1$

Thus,

$$\frac{\delta}{D}=\frac{1}{2}\left[1-(1-\varepsilon_F)^{0.5}\right] \tag{16}$$

where ε_F is the film fraction and $\frac{\delta}{D}$ is the dimensionless liquid film thickness.

The probes were located at various sections of the pipe: 17 and 21 pipe diameters, upstream and downstream of the bend, respectively, and at 45°, 90°, and 135°. This enabled the determination of the PDF of dimensionless liquid film thickness to be obtained.

A typical time series and PDF of dimensionless liquid film thickness before, around and after the 180° return bend at liquid and gas superficial velocities of 0.2 and 14.2 m/s, respectively are presented in Fig. 6. From an analysis of the time series and PDF of dimensionless liquid film thickness, the flow pattern upstream of the bend is confirmed to be churn flow. This was also verified by visual observation. On entering the 45° bend, the centrifugal force displaces the liquid to the outside of the bend, whilst the gas migrates to the inside of it. Gravity on the other hand, drains part of the liquid to the inside of the bend. The flow pattern within this vicinity is annular flow. However, the gas–liquid interface is wavy as shown from the time series of dimensonless liquid film thickness (Fig. 6). As the air–water flow enters the 90° bend, the orientation of the flow changes from the vertical to horizontal and hence gravity slows them down and drains more of the liquid to the bottom of the bend. From an analysis of the time trace of the dimensionless liquid film thickness as shown in Fig. 6, it is concluded that the liquid film is very thick and unstable. Although more waves appear on the gas–liquid film interface, the flow pattern still remains annular. According to Hills (1973) annular flow in horizontal tubes depends on a high level of entrainment to replenish the liquid film at the top of the tube which in turn implies a film of sufficient thickness for entrainment to occur. At the 135° bend, the flow pattern is still annular. On reaching the downcomer, the gas is now at the centre of the pipe whilst the liquid moves to the walls of the pipe. Here, the liquid film is thick due to the fact that the effect of gravity on the two-phase flow is greatest: both gravity and flow are in the same direction whilst buoyancy is in the opposite direction. However, the flow pattern is still annular.

An analysis of the plots of the time series of dimensionless liquid film thickness for the riser, 45°, 90°, 135° and downcomer as depicted in Fig. 6 and Table 3 shows that:

Riser: Fifteen peaks may be seen in the 10 s sample illustrated. These can be interpreted as waves on a base film. These waves are created due to the high gas shear stress acting at the gas–liquid interface. The waves are able to remain on the gas–liquid interface because the gas inertia is able to overcome the gravitational force which may want to collapse them.

(a) Some of the waves at the 45° bend position merge with one another and so create larger ones. However, the value of the highest peak of the waves as shown in Table 3 remained the same, 3.06 mm. However, the number of visible waves in the 10 s sample goes down to 9. It can be observed from Fig. 6 and Table 3 that the drop in the liquid film thickness suggests that some of the liquid could not climb up the bend due to the influence of gravity and as a consequence falls back into the riser (back flow).

(b) Moving from the 45° to 90° position shows that there is an increase in the coalescence of waves leading to larger ones. The values of the peaks of the waves have now decreased further to 2.18 mm, whilst the height of the liquid film as shown in Table 3 has increased to 0.41 mm. The ratio of the wave height to the average liquid film thickness has now decreased to 5.38. This is close to the value of 4–6 obtained by Hewitt and Nicholls (1969).

(c) The mean height of the liquid film thickness at 135° has increased to 0.61 mm. The number of peaks has decreased to six. It is interesting to note that the waves are very thick having a maximum peak of 2.22 mm with a large base superimposed on the dimensionless liquid film thickness traces. The thick liquid film observed is due to the accumulation of liquid at the bottom of the pipe. The ratio of wave height to average liquid film thickness has decreased further to 3.65.

(d) Due to the force of gravity acting in the same direction as the flow, some of the waves are being broken down on entering the downcomer. The appearance of the waves in the downcomer is not as clear as compared to others.

3.3. Variation of mean film fraction with gas superficial velocity

Following these studies attempts have been made to understand the effect of 180° return bend on the film fraction. Fig. 7 (a–e) shows the variation of the average film fraction with the gas superficial velocity for different liquid superficial velocities. A comparison of the outputs of the conductance ring probes are made for the five different locations, riser, 45°, 90°, 135° and the downcomer. It can be concluded that there is a general trend that the average film fraction over the cross-sectional area for the bend flow is lower than that for an upward vertical flow. This is because at the bend the slip is less than that of a straight pipe. Similar observation was also reported by Usui et al. (1983) who worked on an inverted 180° bend using air–water as the model fluids. The average film fraction is found to decrease slightly for gas superficial velocity from 6 to 10 m/s, and above 10 m/s becomes practically constant regardless of the measurement location. The study also found out that the average film fraction for the riser was generally greater than for the downcomer at low gas superficial velocity. The difference between the values of the average film fractions, riser and downcomer decreases as the gas superficial velocity increases. This is to be expected since in downward flow (downcomer) the buoyancy force is acting on the gas phase in a direction opposite to the main flow, while in upflow it complements the main flow. The effect is such that the actual gas velocity is mostly greater in upward flow than in downward flow. This results in a higher film fraction for upward flow (riser) for the same liquid and gas superficial velocities.

It can be observed in Fig. 7 that at liquid superficial velocity of 0.02 m/s, a maximum average film fraction of 0.062 is obtained for the riser at gas superficial velocity of 6.2 m/s. However, the maximum value obtained decreased to a minimum at the 135° bend due to entrainment of droplets arising from the shearing off of the crest of waves. It is interesting to observe that as the gas

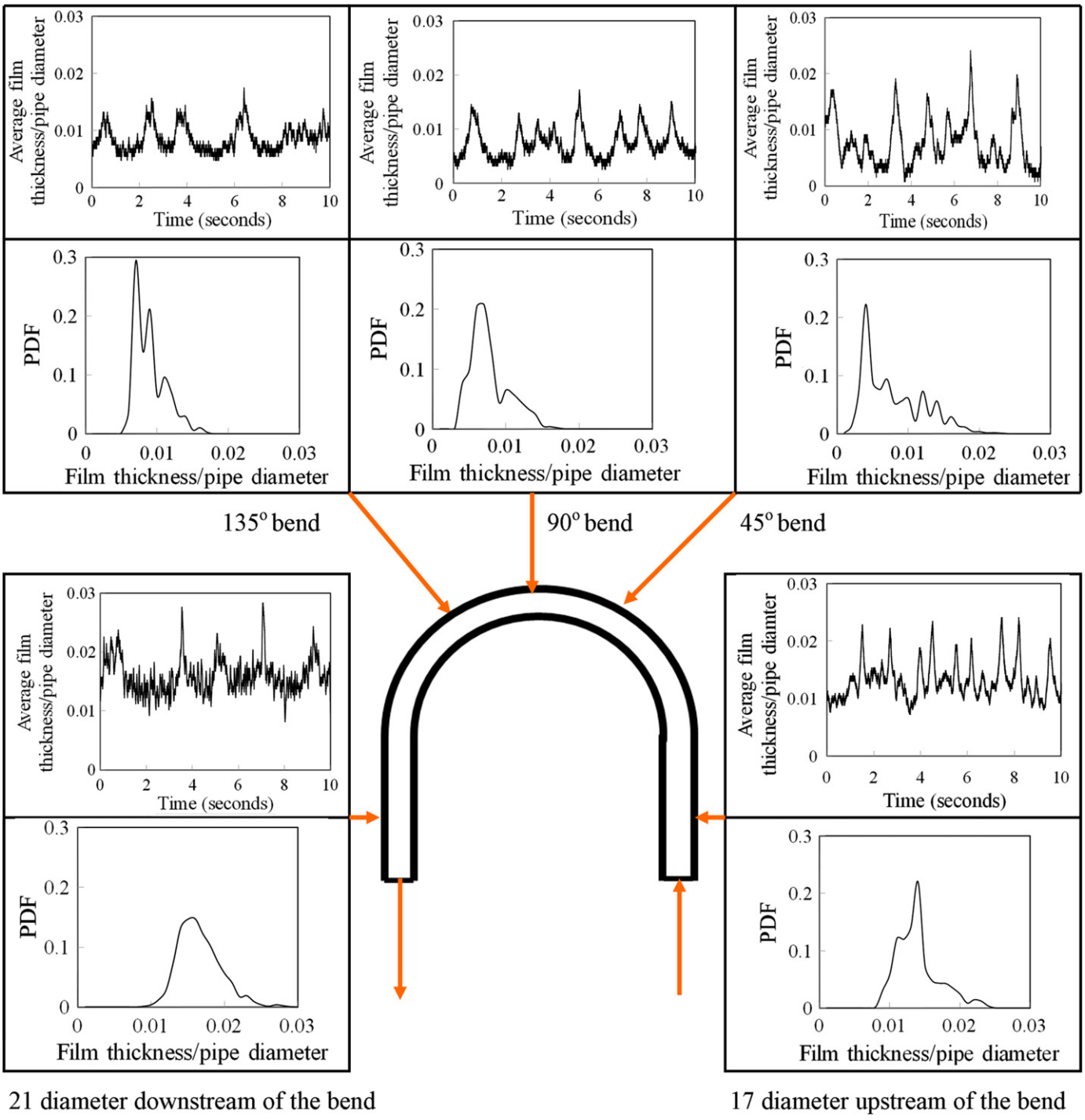

Fig. 6. A typical time series and PDF of dimensionless liquid film thickness around the 180° return bend for liquid and gas superficial velocities of 0.2 and 14.22 m/s, respectively.

Table 3
Mean height of liquid film, ratio of maximum peak height to film mean height and frequency of peak appearance.

	17 pipe diameter (upstream)	45°	90°	135°	21 pipe diameter (downstream)
Mean height of the liquid film (mm)	0.94	0.10	0.41	0.61	1.10
Ratio of maximum peak height to film mean height	3.26	30.13	5.38	3.65	3.25
Frequency of peak appearance	15.0	9.0	7.0	6.0	6.0

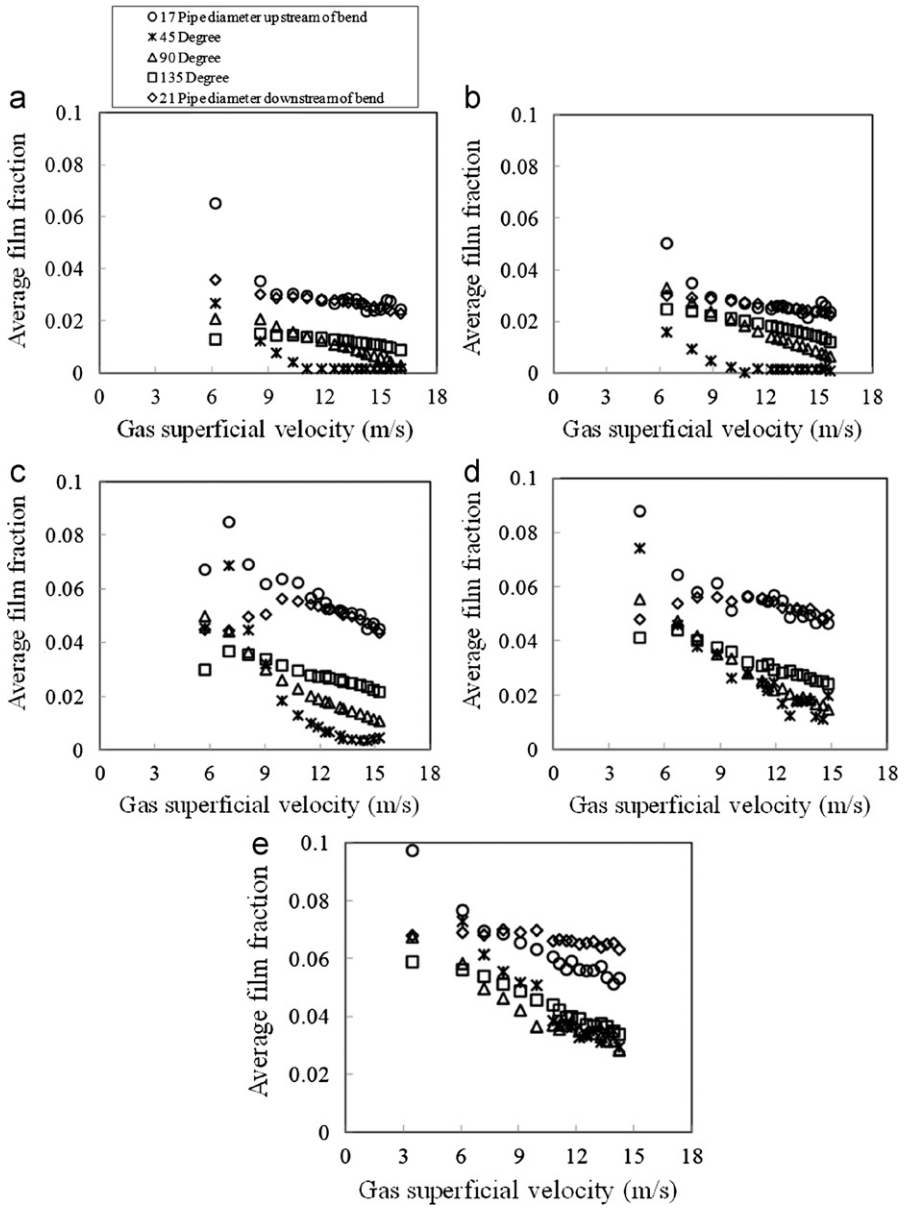

Fig. 7. Variation of average film fraction with gas superficial velocity before, around and after the 180° return bend at liquid superficial velocity of (a) 0.02 m/s (b) 0.04 m/s (c) 0.08 m/s (d) 0.1 m/s and (e) 0.2 m/s.

superficial velocity is increased from 6.2 to 9 m/s, the value of the average film fraction for both the riser and downcomer become the same and continued in that manner throughout the remaining gas superficial velocities studied. This shows that the film fraction is less sensitive to the flow direction in those regions. Therefore, this signifies that the gas superficial velocity of 9 m/s may be regarded as the critical gas velocity, for the direction of flow to be insignificant. For the bend pipe section, at the higher gas superficial velocities, the maximum and minimum average film fractions are observed at the 135° and 45° bend locations, respectively. It is interesting to observe that the average film fraction for the 45° at gas superficial velocity of 10.5 to 15 m/s and liquid superficial velocity of 0.02 m/s is almost zero, suggesting that there is a film breakdown within the vicinity. The film breakdown (burn out) phenomenon is clearly the result of a total loss of water from the liquid film by evaporation and entrainment. This is similar to the observation reported by Balfour and Pearce (1978) and Poulson (1991) with regards to film breakdown. This is also in agreement with the works of Hewitt and Lacey (1965) and Hills (1973) who investigated the breakdown of thin liquid films in climbing film flow. They concluded that with low liquid rates the film can exist in a metastable condition and that if breakdown is induced artificially then the dry patch so formed will not re-wet unless the liquid flow rate is increased considerably.

If the liquid superficial velocity is doubled at a gas superficial velocity of 6.4 m/s, the maximum average film fraction is observed at the riser whilst values at the 45° into the bend are the smallest. The (riser and downcomer) and the 45° bend are observed to have the maximum and minimum average film fractions, respectively at higher gas superficial velocities. The same observation made for the case of liquid superficial velocity of 0.02 m/s is also seen here with regards to the riser and downcomer; at gas superficial velocity of 9.2 to 15.6 m/s, the average film fraction becomes almost the same. Also observed here is the film breakdown within the 45° bend at higher gas superficial velocities.

At liquid superficial velocity of 0.08 m/s, the point of convergence of the riser and downcomer moved to about 12 m/s.

The minimum average film fraction is observed for the 45° followed by the 90° bend. This is due to the fact that some of the liquid films are not able to move into the bend. This is because gravity has a significant effect on the liquid film; the liquid becomes thicker within that vicinity and as a consequence result in a backflow. A similar trend is observed when the liquid superficial velocity is increased to 0.1 m/s. Though, there is an absence of film breakdown in the 45° bend at higher gas superficial velocities.

When the liquid superficial velocity is increased to 0.2 m/s and at gas superficial velocity of 6.2 m/s, the value of average film fraction is almost the same for both the riser and the downcomer. Though, initially, the value of the average film fraction was higher in the riser than the downcomer at gas superficial velocity of 3.5 m/s. It can be concluded that at liquid and gas superficial velocities of 0.2 and 6.2 m/s, respectively, the 180° return has no effect on the flow. An interesting observation made in this study is that as the gas superficial velocity is increased to about 9 m/s, the average film fraction starts to diverge; the point of maximum average film fraction is shifting from the riser to the downcomer. It is this shift in the location of the maximum average film fraction from maximum to minimum that is called film inversion. The film inversion becomes apparent at higher gas superficial velocities. This seems to suggest that the influence of flow direction and entrainment are becoming significant. This is because we have more gas entrainment in the riser than in the downcomer. The location of the minimum average film fraction in the bend however, is not very clear. The maximum average film fraction is observed to be in the 135° bend, followed by the 45° then the 90° bend. The explanation for this is: large droplets with a velocity similar to that of the gas and with a density similar also to that of water moving at the gas speed are deposited at the outside of the bend by centrifugal forces. When these droplets hit the outside of the bend, they are converted into liquid film and spread in different directions, including the downcomer and 135° into the bend. This could explain why we have thickening of liquid film in the 135° bend.

Although this presentation is useful for giving an idea of how, in a mean sense, the liquid film varies with the gas superficial velocity before, within and after the bends, it is not easy to quantify the information. For this reason, the experimental average film fraction data will be presented in terms of axial distance.

3.4. The effect of gas superficial velocity on mean film fraction

Fig. 8 shows the effect of gas superficial velocity on average film fraction at different axial distance. On the plot, −2159 mm, −299 mm and 0 mm represent 17 pipe diameters upstream of the bend, 45° and 90°, respectively. On the other hand, 299 and 2667 mm correspond to 135° and 21 pipe diameters downstream of the bend. Here, the axial distance expressed in mm has a negative sign for upstream of the bend, and a positive sign for downstream of it. For the sake of clarity, the points belonging to the same liquid and gas superficial velocities are joined by dash lines. In order to check the effect of gravity on flow, a straight line is used to join the average film fraction obtained at the riser and the downcomer positions. The figure shows the location of the maximum and minimum average film fractions around the bend.

One interesting observation made in this study is that gravity has no effect on the flow at the highest gas superficial velocities over the range of liquid superficial velocities studied 0.02–0.2 m/s. This is based on the fact that the average film fraction for the riser and downcomer are almost same.

At liquid and gas superficial velocities of 0.02 and 6.2 m/s, respectively, the average film fraction decrease linearly from (0.0653 to 0.012) with axial distance (−2159 to 299 mm). It then increased to 0.0359 at 2667 mm. As the gas superficial velocity is increased to 8.6 m/s, the position of minimum average film fraction shifts to −299 mm whilst the location of maximum average film fraction is still at −2159 mm. Contrary to this at gas superficial velocity of 13.3 m/s, the minimum average film fraction is obtained at −299 mm. This suggests that further proportions of gas as the fluid moved from the −2159 to −299 mm in relation to liquid flow rate led to the occurrence of film inversion.

When the liquid superficial velocity is doubled and at gas superficial velocity of 6.4 m/s, the locations of minimum and maximum values of average film fraction are 299 and −2159 mm, respectively. At gas superficial velocity of 8.9 m/s, the average film fraction decreased from 0.03 at −2159 mm to 0.005 at −299 mm. It recovered to 0.0239 at 0 mm, dropped a little at the 299 mm before finally increasing to 0.0289 at 2667 mm. At the maximum gas superficial velocity of 15.6 m/s, the minimum and maximum average film fractions are observed at the −299 and −2159 mm, respectively. It then increased linearly to 0.0122 at 299 mm before finally increasing to 0.0289 at 2667 mm.

The positions of the minimum and maximum average film fraction at liquid and gas superficial velocity of 0.08 and 5.7 m/s respectively, are at −2159 and 299 mm, respectively.

It can be concluded that the maximum average film fraction is observed at the lowest gas superficial velocity for different liquid superficial velocities except at liquid superficial velocity of 0.08 m/s, where the value is obtained at the second lowest gas superficial velocity, 8 m/s. The location of maximum average film fraction is observed contrary to the −2159 mm to be at −299 mm for the highest liquid superficial velocity. This shows that the liquid has strong influence in the flow behaviour.

It can be concluded in general that the liquid and gas flow rates, gravity and centrifugal forces have a strong effect on the flow behaviour in a 180° return bend.

3.5. Competition between gravitational and centrifugal forces

Oshinowo and Charles (1974) and Usui et al. (1983) proposed a criterion based on a modified form of Froude number, *Fr*, to determine positions of the liquid within the 180° return bend. According to their proposed criterion when *Fr* is greater than 1, the liquid will move outside the bend whilst for *Fr* less than unity, the liquid will hug to the inside of the bend. The validity of the criterion will be discussed here based on the fact that the test bend is located in a vertical plane so that the flow passes from vertical upflow to vertical downflow. It is worth mentioning that in the present study the densities of the liquid and gas are 998 and 3.55 kg/m^3, respectively. Based on the densities of both phases, the ratio of the gas and liquid superficial velocities was determined as follows:

The centrifugal force needed to confine unit volume of fluid to move in a circular path or radius of bend R for both the liquid and air, F_l and F_g, respectively can be, represented as:

$$F_l = \frac{\rho_{Liquid} {u_{ls}}^2}{R} \tag{17}$$

$$F_g = \frac{\rho_{Gas} {u_{gs}}^2}{R} \tag{18}$$

At equilibrium, $F_l = F_g$

$$\frac{\rho_{Liquid} {u_{ls}}^2}{R} = \frac{\rho_{Gas} {u_{gs}}^2}{R} \tag{19}$$

where $u_{gs}$and u_{ls}, the gas and liquid superficial velocities, respectively.

$$\rho_{Liquid} {u_{ls}}^2 = \rho_{Gas} {u_{gs}}^2 \tag{20}$$

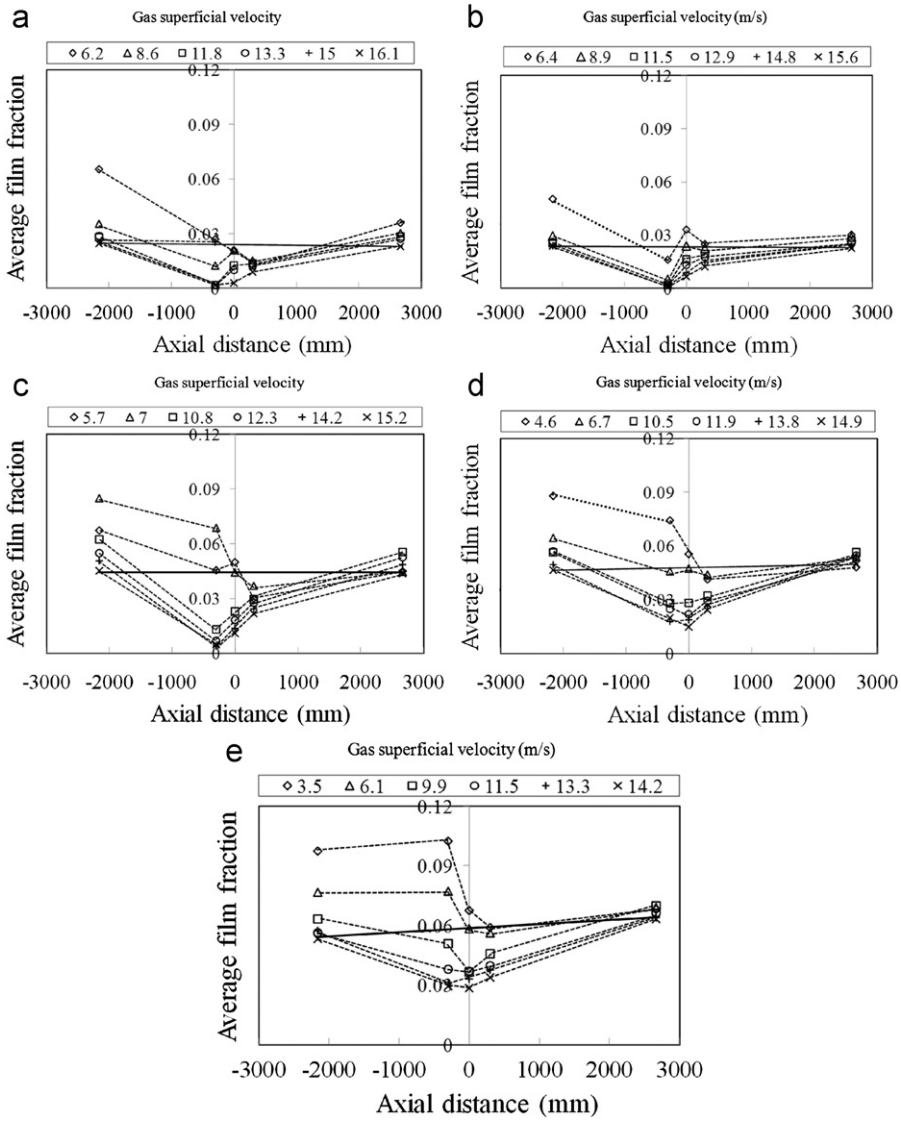

Fig. 8. Variation of average film fraction with axial distance before, around and after the 180° return bend at liquid superficial velocity of (a) 0.02 m/s (b) 0.04 m/s (c) 0.08 m/s (d) 0.1 m/s and (e) 0.2 m/s.

But,

$$\frac{u_{gs}}{u_{ls}} = \sqrt{\frac{\rho_{Liquid}}{\rho_{Gas}}} = \sqrt{\frac{998}{3.55}} = 16.8$$

Therefore,

$$u_{gs} = 16.8 \times u_{ls}\ m/s \tag{21}$$

Eq. (21) therefore represents the ratio of gas and liquid superficial velocities. This means that the liquid will have a higher momentum flux than the gas unless the velocity of the latter is 16.8 times greater.

The condition for which the liquid goes to the outside or inside of the bend are identified in Fig. 8 as modified form of Froude number plotted against gas superficial velocity with liquid superficial velocity as a parameter. There was one combination of flow rate (Froude number equals to 1) where it was not clear whether it was liquid or gas which was on the outside of the bend. For flow rates which give a low Froude number, the flow patterns in the riser approaching the 135° bend through the 45° and 90° bends is annular flow. The gas superficial velocity is greater than that for the liquid. As the liquid density is much greater than that for the gas, gravity dominates and we would expect the liquid to move to the inside of the 45°, 90° and 135° bends, as in fact observed. Conversely, when the modified form of Froude number is negative it tells us that the liquid is being driven to the inside of the bend independently of gravity. For churn flow, the gas superficial velocity is much greater than that for the liquid. Again the liquid density is much greater than that for the gas, the modified form of Froude number is >1 and we would expect the liquid to move to the outside of the 45° bend, as in fact observed. As both the mixture move from the 90° to the 135° bend through the 45° bend, gravity slows them down and throws the liquid to the bottom of the bend and the gas to the outside (Fig 9).

3.6. Comparison of the present work with that of Usui et Al. (1983) flow pattern map

Usui et al. (1983) developed a flow pattern map for an inverted 180° bend based on the basis of visual observation. They claimed that the flow patterns which were observed in the bend were generally similar to those for the C-shaped bend flow except the ways of the gas and liquid distributions and the shape of the bubbles. The map is shown in Fig. 10, indicating the form of the

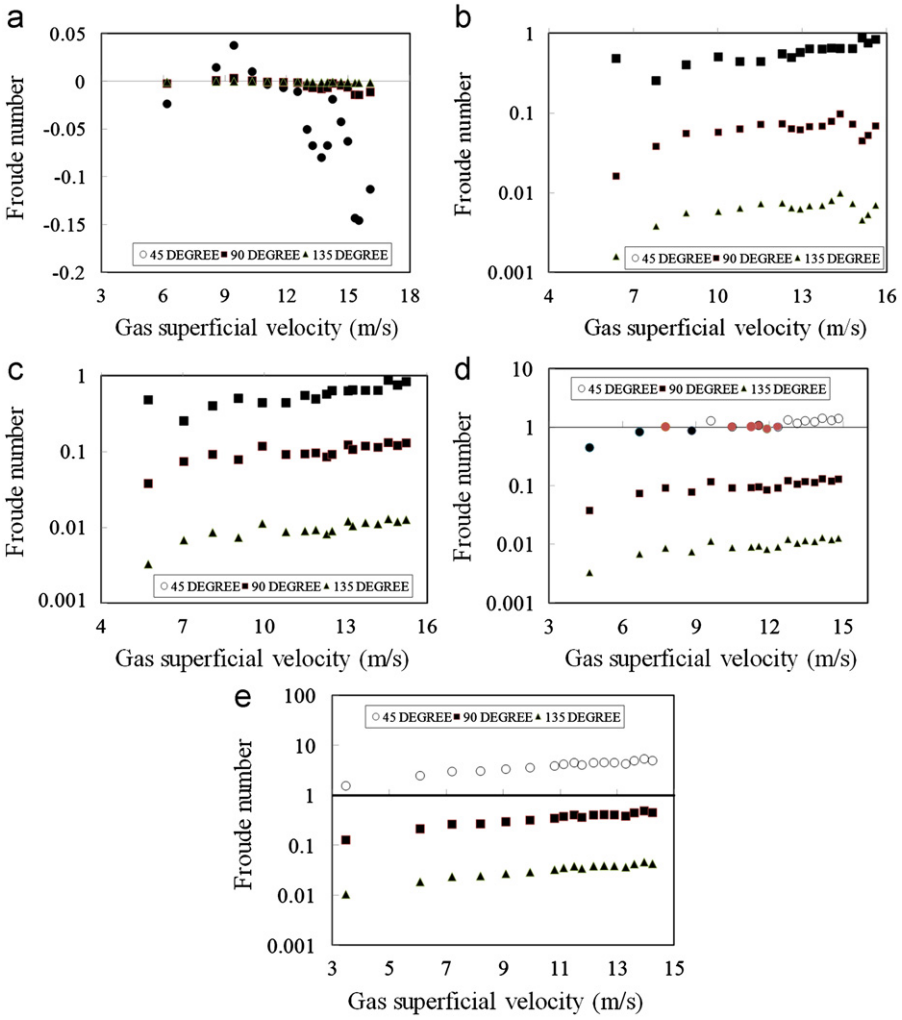

Fig. 9. Influence of gas superficial velocity on the modified Froude number for different liquid superficial velocities of (a) 0.02 m/s (b) 0.04 m/s (c) 0.08 m/s (d) 0.1 m/s and (e) 0.2 m/s.

flow observed at various combination of liquid and gas superficial velocities. According to the transition boundary lines shown on the map, the flow pattern is annular mist flow for liquid superficial velocity of 0.04 m/s and gas superficial velocity of 15.6 m/s. On the other hand, for higher liquid superficial velocities, 0.08 – 0.2 m/s, annular flow except at the lower and intermediate gas superficial velocities. From the map also, the region above the 90° and 135° lines would correspond to the case where the liquid moves to the outside of the bend, the air shifting to the inside, and the region below the lines would give the opposite. However, they did not show on the map the line for the 45° bend. They concluded that the inverted 180° bend has the effect of extending the region of annular flow toward much lower gas velocities.

In the present work contrary to the Usui et al.'s flow pattern transition boundaries, at liquid superficial velocity of 0.02 – 0.04 m/s, the flow pattern is annular whilst there is a good agreement with the other liquid flow rates, 0.08 – 0.2 m/s except at the high gas superficial velocities. The two lines depicted in the map corresponding to the 90° and 135° are in contradiction to the present work: at the 90° and 135° the liquid moves to the inside of the bend for all liquid and gas flow rates considered.

3.7. *Comparison between present study and that of Hills (1973)*

A comparison between the present study and that of Hills (1973) will be made based on mean film fraction at 45°, 90°, and

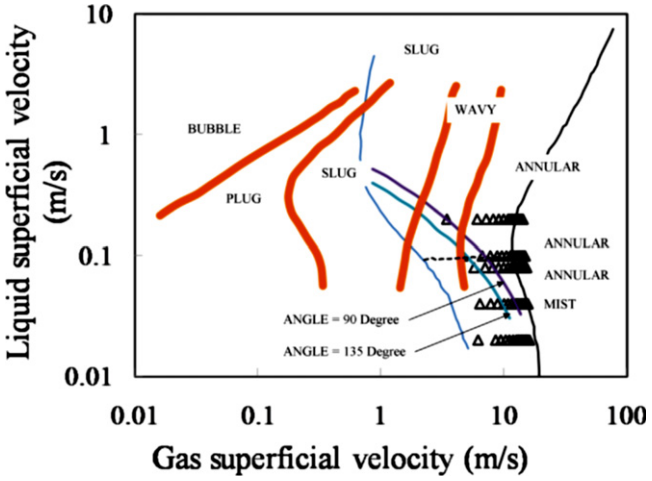

Fig. 10. Flow pattern map of Usui et al. (1983).

135° bends. Hills carried out experimental work on a 180° return bend with pipes of an internal diameter of 25.4 mm. The radius of curvature was 305 mm and the fluids employed were air and water at a system pressure of 1.5 bar absolute. The results of the comparison presented in Fig. 11 were carried out at the same liquid superficial velocity of 0.04 m/s. The plot shows the same

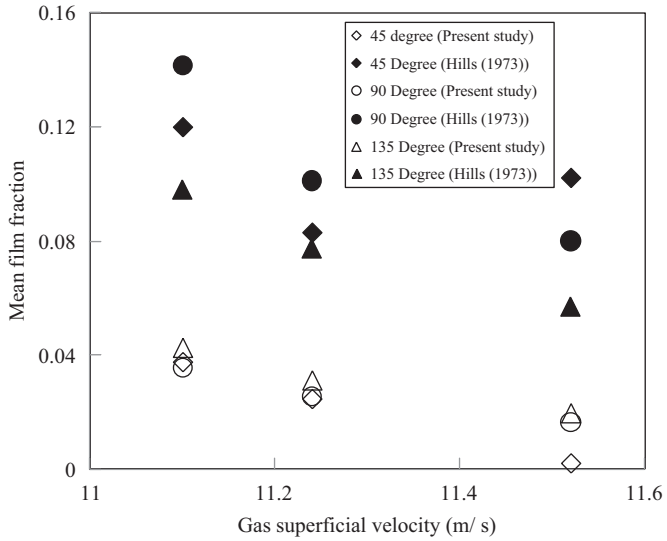

Fig. 11. Comparison of mean film fractions (present study) with those of Hills (1973).

tendency, though the values of mean film fraction obtained from the work of Hills are higher than those of present study. This might be due to the fact that the amount of entrainment of liquid drops in the gas core in large diameter pipe is greater than that of smaller pipes. Therefore there is less liquid in the film in the large diameter case.

4. Conclusions

The experimental study on the influence of a large diameter 180° return bend which is needed in the aspects of operational design and safety of the fired reboiler has been carried out. The observation of two-phase churn-annular flow behaviour and mean film fraction around the bend yielded the following conclusions:

1) A remarkable similarity was observed between the shape of the time series of film fraction, PDF distribution and location of the frequency in the PDF and PSD plots of the three probes.
2) The plot of the time series of dimensionless liquid film thickness at high liquid flow rate revealed the merging and collapsing of waves as they move from the riser to the downcomer through the bends.
3) The average film fraction is found to be higher in the straight pipes than in bends.
4) The study also found that at low gas superficial velocities that the average film fraction for the riser was generally greater than for the downcomer.
5) For low liquid flow rates and high gas superficial velocities, film break down (burn out) occurs at the 45° position around the bend.
6) The study found that the effect of gravity is insignificant at the highest gas superficial velocity.
7) The condition for which the liquid goes to the outside or inside of the bend can be identified based on a modified form of Froude number, a proposal first made by Oshinowo and Charles (1974). A plot of the modified form of Froude number against gas superficial velocities was used to locate position of the liquid in the bend.
8) The plot of liquid superficial velocity versus gas superficial velocity using the Usui et al. (1983) did not give a reasonably good agreement.
9) The comparison between the results of the plot of mean film fraction obtained from the present study and those of Hills (1973) showed the same tendency.

Acknowledgements

M. Abdulkadir would like to express sincere appreciation to the Nigerian government through the Petroleum Technology Development Fund (PTDF) for providing the funding for his doctoral studies.

D. Zhao was funded by EPSRC under grant EP/ F016050/ 1 and A. Azzi held a visiting Research fellowship under the same grant.

The author(s) wish to express their sincere gratitude for this support.

References

Alves, G.E., 1954. Co-current liquid–gas flow in a pipeline contactor. Chem. Eng. Prog. 9, 50.
Asali, J.C., Hanratty, T.J., 1985. Interfacial drag and film height for vertical annular flow. AIChE J. 31, 895–902.
Anderson, G.H. & Hills, P.D., 1974. Two-phase annular flow in tube bends. Symposium on Multiphase flow Systems. University of Strathclyde, Glasgow, Paper J1, Published as Institution of Chemical Engineers Symposium, Series No. 38.
Andreussi, P., Di Donfrancesco, A., Messia, M., 1988. An impedance method for the measurement of liquid hold-up in two phase flow. Int. J. Multiphase Flow 14, 777–785.
Azzopardi, B.J., 1996. Drops in annular two-phase flow. Int. J Multiphase Flow 23, 1–53.
Azzopardi, B.J., 2006. Gas–liquid flows, Begell House.
Balfour, J.D. & Pearce, D.L., 1978. Annular Flows in Horizontal 180° Bends: Measurements of Water Rate Distributions in the Film and Vapour Core. C.E.R.L. Note no. RD/L/N96/78.
Brown, R.C., Andreussi, P., Zanelli, S., 1978. The use of wire probes for the measurement of liquid film thickness in annular gas-liquid flows. Canad. J. Chem. Eng. 56, 754–757.
Chong, L.Y., Azzopardi, B.J., Bate, D.J., 2005. Calculation of conditions at which dryout occurs in the serpentine channels of fired reboilers. Chem. Eng. Res. Des. 83, 412–422.
Coney, M.W.E., 1973. The theory and application of conductance probes for the measurement of liquid film thickness in two phase flow. J. Phys., E: Sci. Instrum. 6, 903–910.
Conte, G., Azzopardi, B.J., 2003. Film thickness variation about a T-junction. Int. J. Multiphase Flow 29, 305–325.
Costigan, G., Whalley, P.B., 1997. Slug flow regime identification from dynamic void fraction measurements in vertical air-water flows. Int. J. Multiphase Flow 23, 263–282.
Fossa, M., 1998. Design and performance of a conductance probe for measuring the liquid fraction in two-phase gas–liquid flows. Flow Meas. Instrum. 9, 103–109.
Gill, L.E., Hewitt, G.F., Hitchon, J.W., Lacey, P.M.C., 1963. Sampling probe studies of the gas core in annular two phase flow-1: the effect of length on phase and velocity distribution. Chem. Eng. Sci. 18, 525–535.
Hewitt, G.F., 1978. Measurements of Two-Phase Flow Parameters. Academic Press, London.
Hewitt, G.F., Lacey, P.M.C., 1965. The breakdown of the liquid film in annular two-phase flow. Int. J. Heat Mass Trans. 8, 781–786.
Hewitt G.F. & Nicholls, B., 1969. Film Thickness Measurements in Annular Flow Two-Phase Flow Using a Fluorescence Spectrometer Technique. UKAEA Report AERE-R4506.
Hills, P.D., 1973. A Study of Two-Phase (Gas–Liquid) Flow in a Tube Bend. Ph.D. Thesis, Imperial College, London.
Hoang, K., Davis, M.R., 1984. Flow structure and pressure loss for two-phase flow in round bends. J. Fluids Eng. 106, 30–37.
James, P.W., Azzopardi, B.W., Graham, D.I. & Sudlow, C.A., 2000. The effect of a bend on droplet distribution in two-phase flow. International Conference on Multiphase Flow in Industrial Plants, Bologna. 13–15 September.
Jayanti, S., Hewitt, G.F., 1992. Prediction of the slug-to-churn flow transition in vertical two-phase flow. Int. J. Multiphase Flow 18, 847–860.
Kaji, R., Azzopardi, B.J., 2010. The effect of pipe diameter on the structure of gas/liquid flow in vertical pipes. Int. J. Multiphase flow 36, 303–313.
Kang, H.C., Kim, M.H., 1992. The development of a flush-wire probe and calibration method for measuring liquid film thickness. Int. J. Multiphase Flow 18, 423–437.
Koskie, J.E., Mudawar, I., Tiederman, W.G., 1989. Parallel wire probes for measurement of thick liquid films. Int. J. Multiphase Flow 15, 521–530.
Miya, M., Woodmansee, D.E., Hanratty, T.J., 1971. A model for roll waves in gas–liquid flow. Chem. Eng. Sci. 26, 1915–1931.
Moffat, R.J., 1988. Describing the uncertainties in experimental results. Exp. Therm. Fluid Sci. 1, 3–17.

Omebere-Iyari, N.K., 2006. The Effect of Pipe Diameter and Pressure in Vertical Two-Phase Flow. Ph.D. Thesis, University of Nottingham.

Oshinowo, T., Charles, M.E., 1974. Vertical two-phase flow—Part 1: Flow pattern correlations. Canad. J. Chem. Eng. 52, 25–35.

Poulson, B., 1991. Measuring and modelling mass transfer at bends in annular flow two-phase flow. Chem. Eng. Sci. 46, 1069–1082.

Sakamoto, G., Doi, T., Murakami, Y. & Usui, K., 2004. Profiles of liquid film thickness and droplet flow rate in U-bend annular mist flow. Fifth International Conference on Multiphase Flow, ICMF 2004, Japan, May 30–June 4.

Shoham, O., 2005. Mechanistic Modelling of Gas–Liquid Two-Phase Flow in Pipes. Society of Petroleum Engineers, USA.

Takemura, T., Roko, Shiraha, M., 1996. Dryout characteristics and flow behaviour of gas-water flow through U-shaped and inverted U-shaped bends. Nucl. Eng. Des. 95, 365–373.

Tsochatzidis, N.A., Karapantsios, T.D., Kostoglou, M.V., Karabelas, A.J., 1992. A conductivity probe for measuring liquid fraction in pipes and packed beds. Int. J. Multiphase Flow 18, 653–667.

Usui, K., Aoki, S., Inoue, A., 1980. Flow behaviour and pressure drop of two-phase flow through C-shaped bend in a vertical plane–I: Upward flow. J. Nucl. Sci. Technol. 17, 875–887.

Usui, K., Aoki, S., Inoue, A., 1983. Flow behaviour and phase distributions in two-phase flow around inverted U-bend. J. Nucl. Sci. Technol. 20, 915–928.

Wang, C.C., Chen, I.Y., Yang, Y.W., Chang, Y.J., 2003. Two-phase flow pattern in small diameter tubes with the presence of horizontal return bend. Int. J. Heat Mass Trans. 46, 2975–2981.

Wang, C.C., Chen, I.Y., Yang, Y.W., Hu, R., 2004. Influence of horizontal return bend on the two-phase flow pattern in small diameter tubes. Exp. Therm. Fluid Sci. 28, 145–152.

Wang, C.C., Chen, I.Y., Lin, Y.T., Chang, Y.J., 2008. A visual observation of the air-water two-phase flow in small diameter tubes subject to the influence of vertical return bends. Chem. Eng. Res. Des. 86, 1223–1235.